# Effects of Inhibitory Feedback in a Network Model of Avian Brain Stem

**Vasant K. Dasika, John A. White, Laurel H. Carney and H. Steven Colburn**

*J Neurophysiol* 94:400-414, 2005. First published Mar 2, 2005; doi:10.1152/jn.01065.2004

*J Neurophysiol* 94: 400–414, 2005.
First published March 2, 2005; doi:10.1152/jn.01065.2004.

# Effects of Inhibitory Feedback in a Network Model of Avian Brain Stem

**Vasant K. Dasika,[1,2] John A. White,[1,3] Laurel H. Carney,[4] and H. Steven Colburn[1,2]**

[1]*Department of Biomedical Engineering,* [2]*Hearing Research Center,* [3]*Center for BioDynamics, Boston University, Boston, Massachusetts; and* [4]*Departments of Biomedical and Chemical Engineering and Electrical Engineering and Computer Science, Institute for Sensory Research, Syracuse University, Syracuse, New York*

Submitted 12 October 2004; accepted in final form 27 February 2005

**Dasika, Vasant K., John A. White, Laurel H. Carney, and H. Steven Colburn.** Effects of inhibitory feedback in a network model of avian brain stem. *J Neurophysiol* 94: 400–414, 2005. First published March 2, 2005; doi:10.1152/jn.01065.2004. The avian auditory brain stem consists of a network of specialized nuclei, including nucleus laminaris (NL) and superior olivary nucleus (SON). NL cells show sensitivity to interaural time difference (ITD), a critical cue that underlies spatial hearing. SON cells provide inhibitory feedback to the rest of the network. Empirical data suggest that feedback inhibition from SON could increase the ITD sensitivity of NL across sound level. Using a bilateral network model, we assess the effects of SON feedback inhibition. Individual cells are specified as modified leaky-integrate-and-fire neurons with time constants and thresholds that vary with inhibitory input. Acoustic sound level is reflected in the discharge rates of the model auditory-nerve fibers, which innervate the network. Simulations show that with SON inhibitory feedback, ITD sensitivity is maintained in model NL cells over a threefold range in auditory-nerve discharge rate. In contrast, without SON feedback inhibition, ITD sensitivity is significantly reduced as input rates are increased. Feedback inhibition is most beneficial in maintaining ITD sensitivity at high-input rates (simulating high sound levels). With SON inhibition, ITD sensitivity is maintained for both interaurally balanced inputs (simulating an on-center sound source) and interaurally imbalanced inputs (simulating a lateralized source). Further, the empirically observed temporal build-up of SON inhibition and the presence of reciprocal inhibitory connections between the ipsi- and contralateral SON both improve ITD sensitivity. In sum, our network model shows that inhibitory feedback can substantially increase the sensitivity and dynamic range of ITD coding in the avian auditory brain stem.

## INTRODUCTION

The submillisecond difference in the time of arrival of sound to the two ears, interaural time difference (ITD), is a critical cue in the localization and processing of sound sources (cf. Blauert 1997). Nucleus laminaris (NL), the avian homologue of the mammalian medial superior olive (MSO), is the first neural center to receive input from the two ears. Fibers from nucleus magnocellularis (NM) project bilaterally and provide phase-locked, glutamatergic, excitatory input to NL. Single neurons in NL show sensitivity to ITD by performing coincidence detection (Jeffress 1948) on the input from left and right NM (Carr and Konishi 1990; Sullivan and Konishi 1984). Empirical data indicate that ITD sensitivity is maintained in NL over a 50-dB range in sound level (Peña et al. 1996). However, simple coincidence models (Peña et al. 1996; Reed and Durbeck 1995) lose ITD sensitivity as the discharge rate of NM fibers monotonically increases threefold or more with sound level (Warchol and Dallos 1990).

Two mechanisms have been demonstrated to maintain ITD sensitivity in models of NL despite variations in sound level. First, synaptic depression has been observed in the NM to NL synapse (Cook et al. 2003; Kuba et al. 2002). When synaptic depression was included in a model of NL, response to ITD was consistent over a threefold range of input discharge rate (Cook et al. 2003). Without depression, however, ITD sensitivity degraded with elevated input rate. A second mechanism that preserved ITD sensitivity in model NL across sound level was the inclusion of inhibitory input. ITD sensitivity was maintained in a model of NL when a sound-level-dependent, feed-forward inhibitory input from the superior olivary nucleus (SON) was included (Peña et al. 1996). In contrast, ITD sensitivity was lost as sound level was increased without the inclusion of SON inhibition. Inhibition was also used in a model of mammalian MSO (Colburn et al. 2004; Zhou and Colburn 2003) to predict ITD-dependent, nonmonotonic, rate-level curves observed empirically (Goldberg and Brown 1969). While Grau-Serrat and colleagues (2003) included feedback inhibition to their biophysically detailed model of NL, the influence of sound-level dependence was not explicitly explored.

Although modeling studies have demonstrated the effects of synaptic depression (Cook et al. 2003) and feed-forward inhibition on ITD sensitivity across sound-level (Colburn et al. 2004; Peña et al. 1996; Zhou and Colburn 2003), this study is the first to examine ITD sensitivity and sound-level dependence in the context of network feedback inhibition observed in the avian brain stem. Anatomy and physiology from the chicken (Monsivais et al. 2000; Yang et al. 1999) indicate a negative-feedback, gain-control role for the SON, which appears to be well suited to maintain ITD sensitivity in NL despite changes in sound level. The SON receives excitation from NL and nucleus angularis (NA) and provides feedback inhibition to NL, NM, and NA (Burger et al. 2005; Lachica et al. 1994; Monsivais et al. 2000; Yang et al. 1999). The SON also projects to contralateral SON, which may serve to decrease the effects of level imbalances[1] to the two sides (Burger

[1] The physical headsize of the chicken is relatively small, producing negligible acoustic interaural level differences in response to low-frequency stimulation. However, interaural middle-ear coupling has been demonstrated to cause significant differences between the levels of the cochlear microphonic signals in each ear (on the order of two times) in response to low-frequency, free-field, off-center tonal stimuli (Hyson et al. 1994).

Address for reprint requests and other correspondence: H. S. Colburn, Dept. of Biomedical Engineering, Boston University, 44 Cummington St., Boston, MA 02215 (E-mail: colburn@bu.edu).

The costs of publication of this article were defrayed in part by the payment of page charges. The article must therefore be hereby marked "*advertisement*" in accordance with 18 U.S.C. Section 1734 solely to indicate this fact.

  

et al. 2005; Lachica et al. 1994; Monsivais et al. 2000). In contrast, the mammalian system is widely believed to have primarily ascending excitation and inhibition to MSO (cf. Grothe 2003).

Physiological data suggest that the SON is suited to perform gain-control. Single neurons in SON appear able to reflect the average discharge rate of their inputs, as they have relatively long time constants (on the order of 30 ms) and excitatory postsynaptic potential (EPSP) durations (Yang et al. 1999). SON inhibition is GABAergic, which has been demonstrated to decrease the time constant in NL and NM neurons (Monsivais et al. 2000; Yang et al. 1999) and increase the threshold in NM neurons (Monsivais and Rubel 2001). GABAergic inhibitory responses are relatively slow, lasting on the order of tens to hundreds of milliseconds (Funabiki et al. 1998; Hyson et al. 1995; Lu and Trussell 2001; Monsivais and Rubel 2001; Monsivais et al. 2000; Yang et al. 1999), in contrast to the rapid (~1 ms long) glutamatergic responses seen in NL, NM, and NA (Raman et al. 1994). In fact the SON-originated, slow GABAergic input has been demonstrated to modulate NL neurons by reducing the amplitude and shortening the temporal duration of the EPSP induced by glutamatergic input (Yang et al. 1999). As we show, the slow modulation of the fast glutamatergic response by GABAergic input from SON is consistent with the presumed role of the SON in maintaining temporal sensitivity in NL and NM, particularly over variations in sound level. SON activity, moreover, modulates the GABAergic inhibitory response. A stronger SON input or a higher rate of SON inputs has been shown to prolong and strengthen the observed inhibitory response (Lu and Trussell 2000; Monsivais et al. 2000; Yang et al. 1999).

Through computational modeling, we investigate the influence of inhibitory feedback from the SON to the rest of the avian auditory brain stem network. Both balanced and imbalanced level conditions are tested because ITD sensitivity has been empirically observed in NL under both conditions (Peña et al. 1996; Viete et al. 1997). Our network model shows that feedback inhibition from the SON can significantly expand the dynamic range of the avian ITD coding system.

## METHODS

We calculated the response of each neuron in the network to a steady-state pure tone of varying level. The network was comprised of single-model neurons that were designed to include the three attributes described in the INTRODUCTION: first, the fast glutamatergic-like membrane depolarizing response, critical for phase-locking in NM and for ITD sensitivity in NL; second, the slow GABAergic inhibitory response to SON inputs (seen in NM and NL); and third, the temporal build-up of this inhibitory response with increasing SON stimulation. A block diagram of the network model connectivity is shown in Fig. 1. The neural connectivity was based on recent knowledge of the ITD pathway of the chicken (Monsivais et al. 2000).

Table 1 provides a summary of the parameter values used for the simulations in this study unless otherwise noted. Parameters were divided into four categories: input parameters, excitatory connection parameters, inhibitory connection parameters, and cell parameters.

### *Input model*

Auditory-nerve (AN) inputs were generally half-second-duration sets of discharge times delivered to model neurons in the network. As in Peña et al. (1996), two categories of inputs were used: nonphase-locked inputs that were delivered to NA and phase-locked-inputs that were delivered to NM. Nonphase-locked inputs were generated by a homogeneous Poisson process with no dead time. For phase-locked inputs, the response of a single input fiber was constructed by assuming a periodic input with frequency $f$, an average discharge rate $R$, and a temporal jitter random variable with a SD $\sigma$. On each period, the probability that an event occurred equaled $R/f$, ($f \geq R$). If an event occurred, it was placed at a phase determined by the temporal jitter added to the specified average phase. The jitter was specified as a zero mean, normal random variable with a SD chosen to provide the desired vector strength (VS), specifically, $\sigma = \sqrt{-2\ln(\mathrm{VS})}/(2\pi f)$. The jitter was statistically independent from period to period. Input refractoriness was modeled by eliminating inputs that were generated within 1 ms of the previous event on that particular fiber. As given in Table 1*A*, $f = 600$ Hz and VS = 0.76 for most of our phase-locked input cases, as in Cook and colleagues (2003). When multiple-fiber inputs were considered, multiple, statistically identical and independent fibers were used.

The discharge rates of phase-locked and nonphase-locked categories of inputs were used to reflect the sound level of the simulated acoustic stimulus. Rate varied over a threefold range (150–450 spikes/s), as in the Cook et al. (2003) model. On a given side (i.e., the

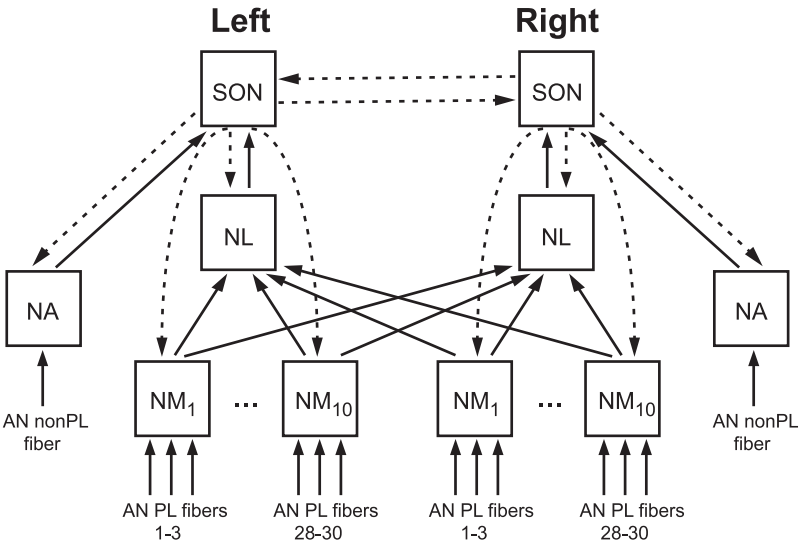


FIG. 1. Network model block diagram. Excitatory connections are shown as solid black lines. Inhibitory connections are shown as dashed lines. One superior olivary nucleus (SON), nucleus laminaris (NL), and nucleus angularis (NA) cell is represented from each of the 2 sides. Ten nucleus magnocellularis (NM) cells are represented per side. Three phase-locked auditory-nerve fibers, "AN PL fibers," innervate each NM cell. Each numbered AN PL fiber on a given side represents 1 independent phase-locked auditory-nerve fiber—all fibers on both sides share the same frequency and vector strength. An independent nonphase-locked auditory-nerve fiber, "AN nonPL fiber", excites each NA cell.

TABLE 1. *Model parameters*

*A. Input parameters*

| | |
|---|---|
| Stimulus duration | 0.5 s [or 2 s] |
| Periodic stimulation frequency (*f*) | 600 Hz [or 450 Hz] |
| AN periodic input vector strength (VS) | 0.76 [or .8] |
| AN input rate | 150, 300, or 450 spikes/s |

*B. Summary of state variables*

| | |
|---|---|
| $V_m$ | membrane voltage |
| $\tau_m$ | membrane time constant |
| $\tau_{\tau_m}$ | time constant that controls the dynamics of the membrane time constant |
| $V_T$ | threshold voltage |
| $\tau_{V_T}$ | time constant that controls the dynamics of the threshold voltage |

*C. Excitatory connections*

| From | To | Syn Delay, ms | $V_m^{inc}$ |
|---|---|---|---|
| AN (phase-locked) | NM | 0 | 1 |
| AN (non-phase-locked) | NA | 0 | 1 |
| NA | SON | 3 | 1 |
| NM | NL | 1.5 or 1.6 | 1 |
| NL | SON | 2 | 1 |
| SON | SON | 5 | 0 [or 1] |

*D. Inhibitory connections*

| From | To | Syn Delay, ms | $\tau_{\tau_m}^{inc}$, ms | $\tau_m^{dec}$, ms | $\tau_{V_T}^{inc}$, ms | $V_T^{inc}$ |
|---|---|---|---|---|---|---|
| SON | NA | 5 | 0 | 0 | 50 | 0.058 |
| SON | NM | 3 | 50 | 0.05 | 50 | 0.068 |
| SON | NL | 5 | 50 | 0.04 | 0 | 0 |
| SON | SON | 5 | 50 | 2 | 50 | 0.125 |

*E. Cell parameters*

| Cell | Abs Refract, ms | $\tau_{\tau_m}^{ceil}$, ms | $\tau_m^0$, ms | $\tau_m^{floor}$, ms | $\tau_{V_T}^{ceil}$, ms | $V_T^0$ | $V_T^{ceil}$ |
|---|---|---|---|---|---|---|---|
| NA | 2 | – | 2 | – | 1000 [or 50] | 1.168 | 2 |
| NM | 1.5 | 1000 [or 50] | 0.417 | 0.2 | 1000 [or 50] | 1.068 | 2 |
| NL | 1 | 1000 [or 50] | 0.8 | 0.3 | – | 3.368 | – |
| SON | 6 | 1000 [or 50] | 40 | 20 | 1000 [or 50] | 2.5 | 5 |

$V_m$, $V_m^{inc}$, $V_T^{inc}$, $V_T^0$, and $V_T^{ceil}$ are all specified in the same relative units. "Syn Delay" represents the combined synaptic and propagation delays. "Abs Refract" represents the absolute refractory period. Dashes represent values that are not necessary since inhibitory input is not specified to affect those states. Entries enclosed in brackets ([ ]) include those tested in a limited number of situations where noted in the paper. AN, auditory nerve; NA, nucleus angularis; NM, nucleus magnocellularis; NL, nucleus laminaris; SON, superior olivary nucleus.

left or the right), the rates for both phase-locked and nonphase-locked inputs were equal. Input rate conditions to the two sides were usually denoted as a pair of rates. For example, "150, 450 spikes/s" means that the rate was 150 spikes/s for the left AN inputs and 450 spikes/s for the right AN inputs.

Pregenerated sets of input times were used for a given stimulus. This made it possible to test the result of different network configurations to the *same* sets of inputs. Consequently, the effects due to changes in the network configuration could be isolated without the additional variability that would occur if different samples of input-time sets were used. Simulations tested responses to driven activity only—spontaneous activity conditions were not tested. Furthermore, only binaural stimulation cases are presented.

## *Network model*

The network model is shown in Fig. 1 with model cells representing NL, NM, NA, and SON on each side. The network was symmetric, with cells and connections on the left side mirroring those on the right side. Three independent, phase-locked auditory-nerve fibers excited each NM cell. Ten separate NM cells were modeled per side, and all 10 NM cells per side bilaterally excited a single NL cell on each side. Different propagation delays could be specified from the NM cells on one side to the left and right NL cells. Each NL cell had a best ITD that was equal in magnitude but opposite in sign to its mirroring NL cell on the other side. The NL cell on each side excited the SON cell on the same side. A single, nonphase-locked, auditory-nerve input fiber from each side excited a single NA cell, and each NA cell excited the SON cell on the same side. Each SON cell inhibited ipsilateral NL, NM, and NA and contralateral SON. Simulations also tested the effects of no SON-feedback inhibition. Where noted in the RESULTS, limited additional simulations tested the effects of other SON-feedback configurations.

The following four subsections describe the structure of a single model cell, the simulation protocol, an overview of the model parameters used, and the data analysis used.

STRUCTURE OF MODEL CELL. Each model cell in the network was an "adapting leaky-integrate-and-fire (LIF)" cell. An adapting LIF cell was defined as a standard LIF cell (cf. Tuckwell 1988) with parameters that were affected by SON input and thereby varied with time.

Consider first a standard LIF cell, which is described by a single state variable, membrane voltage $V_m(t)$. An excitatory input event causes an instantaneous increment $V_m^{inc}$ in membrane voltage. Between inputs, membrane voltage decays toward zero with a fixed membrane time constant $\tau_m$. The differential equation describing the membrane voltage of a standard LIF cell is given by *Eq. 1*

$$\frac{dV_m(t)}{dt} = \frac{-V_m(t)}{\tau_m} + V_m^{inc} \sum_{\text{all } k} \delta(t - t_k) \quad (1)$$

where $\delta(.)$ represents the Dirac delta or impulse function (cf. Dayan and Abbott 2001) and $t_k$ is the time of the $k$th input. The resulting function $V_m(t)$ has the characteristic shape of step increments of height $V_m^{inc}$ at the times of input events with an otherwise continuous exponential decay (with time constant $\tau_m$) to rest (which is normalized to 0 in *Eq. 1*). If the membrane voltage crosses a specified threshold $V_T$, then an output event is generated and the membrane voltage is set to zero and held there for the duration of the absolute refractory period. Figure 2*E* illustrates the response properties of a standard LIF model to the input pattern shown at the *bottom* of the panel, namely: the characteristic shape of $V_m(t)$ (thick black line), the constant threshold $V_T$ (thin black line, equal to 1 here), the membrane voltage reset values (equal to 0), and the refractory period (equal to 1 ms here) following a cell discharge (discharges are indicated at the top of the panel by the × symbols).

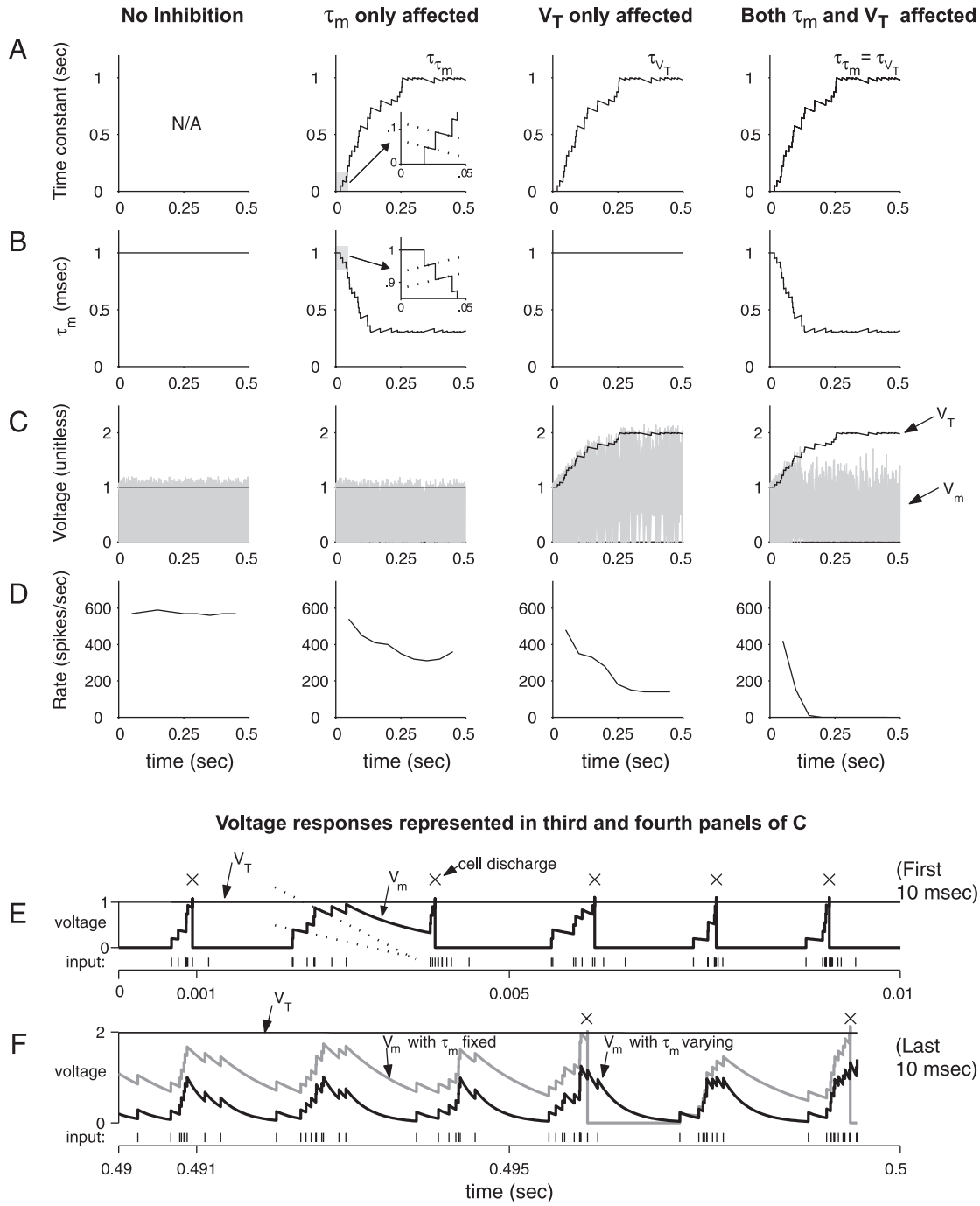


FIG. 2. Illustration of the effects of inhibition on an adapting leaky-integrate-and-fire (LIF) cell model. Four different inhibitory conditions are represented across the four columns in *A–D*. *A*: shows $\tau_{\tau_m}$ and/or $\tau_{V_T}$; *B*: $\tau_m$; *C*: $V_m$ (as the shaded region between the minimum and the maximum voltage values occurring within each stimulus period) and $V_T$; and *D*: the moving-averaged response rates. The same excitatory and inhibitory input time sets were used for each of the 4 inhibitory conditions. *E* and *F*: the details of the voltage responses represented in the *3rd* and *4th panels* of *C*. Input rasters superimposing the 20 independent excitatory inputs are shown below the voltage traces in *E* and *F* (inhibitory input rasters are not shown). Cell discharges are indicated by ×s and shown above the voltage traces. In the 1st 10 ms (*E*), both voltage traces were identical because no inhibitory inputs occurred (the response reflects that of a standard LIF model). In the last 10 ms (*F*), however, the membrane time constant had decreased (as seen in *B*, *4th* vs. *3rd panels*), decreasing $V_m$ (*F,* thick black line) in comparison to when the membrane time constant was unaffected (*F,* thick gray line). Excitatory inputs that occurred within 1 ms of a cell discharge were ignored as a consequence of the specified absolute refractory period. The pairs of dotted lines shown in *E* and in the *insets* of the *2nd panels* of *A* and *B* depict the initial slope of decay at 2 different state variable magnitudes. For this figure: 20 phase-locked inputs excited an adapting LIF cell, each with an average rate of 300 spikes/s. The average rate of the single inhibitory input fiber was 75 spikes/s. No time delays or synaptic delays were added to any of the inputs. An excitatory input caused a depolarization ($V_m^{inc}$) of 0.2 to the membrane voltage, the initial threshold voltage $V_T^0$ was 1, $V_T^{inc}$ was 0.05, and $V_T^{ceil}$ was 2. The refractory period was 1 ms.

The *adapting* LIF model used in the present study extended the standard LIF model such that inhibitory input from the SON elicited changes in the time constant $\tau_m$ and the threshold $V_T$. Based on empirical observations described in the INTRODUCTION, we assumed that SON inhibitory input decreased the membrane time constant $\tau_m$ and increased the threshold $V_T$. Note that both of these changes would

reduce the spike rates of the affected neurons. In addition, as greater SON input has been shown empirically to cause longer lasting changes in NL and NM cell response, we assumed that SON input also increased the recovery times of these two parameters ($\tau_m$ and $V_T$), prolonging the inhibitory response. Otherwise the adapting LIF model operated analogously to the standard LIF model. Excitatory inputs only affected the membrane voltage and did not affect the time constant or the threshold.

Except for a few test cases which are noted in RESULTS, we generally assumed that SON inputs did not directly affect the membrane voltage. The predominant effect of SON input has been empirically demonstrated to be inhibitory (cf. INTRODUCTION), although depolarizing (Hyson et al. 1995; Lu and Trussell 2001; Monsivais and Rubel 2001). GABAergic input from SON opens chloride channels and thereby both decreases the membrane resistance and depolarizes the cell due to chloride efflux (Lu and Trussell 2001; Monsivais and Rubel 2001; Monsivais et al. 2000). Membrane depolarization opens low-voltage-activated potassium channels, further decreasing the membrane resistance (Monsivais et al. 2000). Depolarization also inactivates voltage-dependent inward (e.g., sodium) currents, increasing the voltage threshold for spiking (Monsivais and Rubel 2001). Because ion channels were not explicitly described in the adapting LIF model, the empirically observed effects of: GABA-induced opening of chloride channels, the resulting membrane depolarization, opening of low-voltage-activated potassium channels, and inactivation of inward currents, were specified entirely by the net effects of decreasing the membrane time constant and increasing the voltage threshold, *without* directly changing the membrane voltage. The effects of inhibition in model adapting LIF cells were specified this way because membrane depolarization always moves the cell *closer* to threshold, which would be inconsistent with the empirical observations showing that GABAergic input can move NM cells *away* from threshold.

*State variables.* The adapting LIF model was described by five state variables: the membrane voltage $V_m$, the membrane time constant $\tau_m$, the time constant $\tau_{\tau_m}$ that controlled the dynamics of the membrane time constant, the threshold voltage $V_T$, and the time constant $\tau_{V_T}$ that controlled the dynamics of the threshold voltage. In general, when SON inputs were received, $\tau_m$ decreased so that $V_m$ decayed more quickly. Additionally, $V_T$ increased, making $V_m$ even less likely to cross threshold. SON input also caused $\tau_{\tau_m}$ and $\tau_{V_T}$ to increase so that $\tau_m$ and $V_T$ recovered more slowly. The three effects, decreasing $\tau_m$, increasing $V_T$, and slowing the recovery of $\tau_m$ and $V_T$, modeled the influence of SON inhibition on a target cell, which ultimately decreased cell excitability and firing rate. The state variables of the adapting LIF model are summarized in Table 1B.

Figure 2 illustrates the response of an *isolated* adapting LIF cell model to excitatory (600 Hz, phase-locked) and inhibitory (75 spikes/s, nonphase-locked) inputs. The *left-column panels* of Fig. 2, *A–D*, show the response of a standard LIF cell (without inhibition). The *first* (leftmost) *panel* in *C* shows that the membrane voltage $V_m$ consistently exceeded the threshold $V_T$ on each stimulus cycle in response to the excitatory 600-Hz inputs, causing a relatively constant response rate of ~600 spikes/s (*D*, *1st panel*). However, when inhibition either reduced $\tau_m$ (*2nd column*), increased $V_T$ (*3rd column*), or both (*4th column*), significant decreases in the likelihood of the membrane voltage crossing threshold occurred (see *C*, *2nd–4th panels*). The consequent decrease in the response rate can be seen in the rate-versus-time plots in *D*. The specification of the model state variables is described in the following paragraphs.

We describe in detail the behaviors of $\tau_{\tau_m}$ and $\tau_m$ only. According to our assumptions, the effects of inhibition on the threshold $V_T$ were similar to the effects on the membrane time constant $\tau_m$ so that the discussion about $\tau_m$ is easily translated to $V_T$. The recovery time constant $\tau_{\tau_m}$ of the membrane time constant $\tau_m$ is shown in *A* and was described by two parameters: a (positive) increment amount $\tau_{\tau_m}^{inc} = 50$ ms, and a ceiling value $\tau_{\tau_m}^{ceil} = 1$ s. The membrane time constant $\tau_m$ shown in row B depended on the state variable $\tau_{\tau_m}$, together with three parameters: an initial value $\tau_m^0$, a decrement amount $\tau_m^{dec}$, and a floor value $\tau_m^{floor}$.

The effect of inhibitory inputs on $\tau_m$ are illustrated in Fig. 2, *second column.* The *second panel* in *A* shows that $\tau_{\tau_m}$ was instantaneously incremented by the amount $\tau_{\tau_m}^{inc}$ (50 ms) at the times of inhibitory inputs (the *inset* shows the 1st 50 ms of the trace). Whenever $\tau_{\tau_m}$ was incremented by inhibitory input, the membrane time constant $\tau_m$ (*B, 2nd panel*) was *decremented* by the amount $\tau_m^{dec}$ (equal to 0.05 ms here) from its initial value of $\tau_m^0$ (equal to 1 ms here). Ceiling and floor values were imposed to limit state variable excursions: if $\tau_{\tau_m}$ ever was incremented beyond $\tau_{\tau_m}^{ceil}$ (1 s), it was set equal to $\tau_{\tau_m}^{ceil}$; likewise, if $\tau_m$ ever was decremented to be less than $\tau_m^{floor}$ (equal to 0.3 ms here), it was set equal to $\tau_m^{floor}$.

Between inhibitory inputs, both $\tau_{\tau_m}$ and $\tau_m$ decayed exponentially toward their initial values (0 and $\tau_m^0$, respectively), both with a time constant *equal* to the value of $\tau_{\tau_m}$ immediately after the most recent inhibitory event. As shown in the *insets* of *A* and *B, second panel,* after the first inhibitory input event, both $\tau_{\tau_m}$ and $\tau_m$ recovered exponentially with a time constant equal to 50 ms. After the second inhibitory input, these state variables recovered with a *larger* time constant (which was equal to 92 ms in this example based on the updated value of $\tau_{\tau_m}$). The specified form of $\tau_{\tau_m}$ caused the initial slope of decay of $\tau_m$ and $\tau_{\tau_m}$ to be *independent* of the magnitude of the state variables. This is illustrated by the pair of dotted lines shown in the *insets* of *A* and *B, second panel,* where each line depicts the initial slope of decay immediately following inhibitory input. Within a given panel, both dotted lines followed the *same* initial slope of decay, making the lines parallel. This specified increase of the recovery time constant $\tau_{\tau_m}$ due to inhibitory input provided a simple quantitative description for the empirically observed temporal build-up of inhibitory response (Yang et al. 1999). In contrast, as illustrated by the pair of dotted lines in *E,* a *fixed* time constant exponential response has an initial slope of decay that is *proportional* to the magnitude of the state, causing a fixed decay-time that is independent of state magnitude. A fixed-time-constant model does not exhibit temporal build-up.

*Inhibitory modulators.* In our model, stronger inhibition could be modeled as a larger $\tau_m^{dec}$ parameter which would cause a larger decrement in $\tau_m$ due to an SON inhibitory input. With ongoing inhibitory input, a smaller $\tau_m^{floor}$ value could allow $\tau_m$ to decrease further. Dynamics also affect the strength of inhibition. A SON input increases $\tau_{\tau_m}$ by the amount $\tau_{\tau_m}^{inc}$. A larger value of $\tau_{\tau_m}^{inc}$ increases the duration of the inhibitory response because $\tau_m$ decays exponentially with a time constant equal to the latest incremented value of $\tau_{\tau_m}$. Ongoing SON input causes summation in $\tau_m$ and $\tau_{\tau_m}$, increasing both the magnitude and duration of the inhibitory response. Moreover, the amount of summation is largest when $\tau_{\tau_m}^{ceil}$ is large relative to the (instantaneous) value of $\tau_{\tau_m}$, furthering the temporal build-up. The ceiling value of $\tau_{\tau_m}$ can consequently affect the duration and magnitude of the inhibitory response (see RESULTS).

A substantial, steady rate of inhibitory input as used in Fig. 2 could cause a significant change in both $\tau_m$ and $\tau_{\tau_m}$ over time. As illustrated in the *second* and *fourth panels* of Fig. 2*B*, $\tau_m$ was decreased toward and maintained at its floor value (0.3 ms) as $\tau_{\tau_m}$ (Fig. 2*A*) was increased toward and maintained at its ceiling value, slowing the recovery of both states. Because the value of the membrane voltage $V_m$ was dependent on $\tau_m$, the likelihood of $V_m$ to exceed threshold decreased as $\tau_m$ decreased (compare the *1st* and *2nd panels* in *C;* also, compare the *3rd* and *4th panels* of *C*). Note that similar effects of inhibition can be seen on the threshold, $V_T$, by comparing the *first* and *third* and the *second* and *fourth panels* in *C*.

*Derivation of $V_m$. Equation 2* describes the membrane voltage $V_m$ of the adapting LIF model the membrane time constant $\tau_m$ of which varied with time

$$\frac{dV_m(t)}{dt} = \frac{-V_m(t)}{\tau_m(t)} + V_m^{inc} \sum_{all\ k} \delta(t - t_{exc,k}) \quad (2)$$

where $t_{exc,k}$ is the time of the $k$th excitatory input. (Because excitatory and inhibitory inputs were defined to have different actions in the adapting LIF model, we separately denote their ordered sets of times as $\{t_{exc}\}$ and $\{t_{inh}\}$, respectively.) As described in the preceding text, $\tau_m$ $(t)$ was a piecewise exponential function. A piecewise exponential form for $\tau_m$ $(t)$ was purposefully specified because it enabled us to derive an analytical solution[2] for $V_m$ in *Eq. 2* in terms of $V_m$ at the previous input event. The membrane voltage $V_m$ at some time $t$ after the time of the last input event (whether excitatory or inhibitory at time $t_k$) and before the time of the next input event ($t_{k+1}$), was solved for (see APPENDIX for details), yielding

$V_m(t) = g(t)V_m(t_k^+) \exp(-(t - t_k^+)/\tau_m^0)$ for $t_k^+ \leq t < t_{k+1}$, where

$$g(t) = \left[\frac{\tau_m(t_k^+)}{\tau_m(t)}\right]^{\tau_{\tau_m}(t_{inh,rec}^+)/\tau_m^0} \quad (3)$$

where $t_k^+$ was the time immediately after the last input event, and $\tau_{\tau_m}(t_{inh,rec}^+)$ was the value of $\tau_{\tau_m}$ immediately after the most recent inhibitory event. *Equation 3* is written in a form where the voltage arising from a standard LIF decay, $V_m(t_k^+) \exp[-(t - t_k^+)/\tau_m^0]$, is multiplied by a factor $g(t)$ that was always less than or equal to one. The factor $g(t)$ was less than or equal to one because $\tau_m$ increased toward $\tau_m^0$ between inhibitory inputs (as shown in detail in the *inset* of *B, 2nd panel*). Inhibitory input created a "leakier" cell membrane, which caused the membrane voltage to decay faster than it otherwise would without inhibitory input. As a result, the membrane voltage was generally lower and crossed threshold less often when the time constant varied (*C, 2nd panel*), compared with when the time constant was fixed (*C, 1st panel*), causing a decreased firing rate (*D, 2nd* vs. *1st panel*). Differences were also apparent in the detailed voltage responses resulting from a decreased (Fig. 2*F*, thick black line) versus unaffected (Fig. 2*F*, thick gray line) membrane time constant.

SIMULATION PROTOCOL. Computation of the network response was based on an array of ordered event times. The array initially contained the input times delivered to the network. The array was updated and reordered every time an event was generated within the network. Specifically, after adding appropriate synaptic/propagation delays to the input times, the arrival times at the target cells were ordered in the array. Each array element held the event time, along with the input- and target-cell information associated with that event. The first event was processed, causing all five state variables at the target cell to be updated in ways depending on the specific target-cell/input-cell combination. The target cell was then checked for the occurrence of an output event (an output event occurred if $V_m$ equaled or exceeded $V_T$). If an output event occurred, appropriate synaptic/propagation delay(s) for the current target-cell's target(s) were added, and these time(s) were inserted sequentially in the array. Refractoriness was included in a manner similar to that in a standard LIF model: excitatory inputs arriving at a given cell (which normally incremented the membrane voltage) were ignored for a specified deadtime after the last output at that same cell. During the refractory period, however, inhibitory inputs were processed as usual (i.e., $\tau_{\tau_m}$, $\tau_m$, $\tau_{V_T}$, and $V_T$ were decaying and were incremented whenever inhibitory inputs occurred). The next occurring temporal event in the array was then processed. This update cycle was continued until a specified simulation duration was reached.

[2] An analytical solution was convenient because $V_m$ needed to be calculated only at the time of inputs.

PARAMETERS. The increment and ceiling values for the time constants $\tau_{\tau_m}$ and $\tau_{V_T}$ were generally specified as 50 ms and 1 s, respectively, based on empirical data of NL responses when SON was stimulated (Yang et al. 1999). Additional simulations (see RESULTS) tested values other than 1 s for the ceiling values of the recovery time constants (e.g., ceiling values of 50 ms were specified to fix the recovery time constants at 50 ms).

SON cell parameters were based on in vitro data (Yang et al. 1999). NL parameters were based on in vitro data (Reyes et al. 1996; Yang et al. 1999). NM cell parameters were based on in vivo (Joris et al. 1994) and in vitro (Reyes et al. 1994) data. Finally our specification of NA parameters was consistent with in vitro data (Soares et al. 2002) and elicited a discharge rate range that was compatible with that observed in vivo (Warchol and Dallos 1990).

In most of our network simulations, the right NL was modeled as having a best delay of +100 $\mu$s, i.e., inputs arrived coincidently at the right NL when the right side inputs were delayed by 100 $\mu$s compared with the left side inputs. The left NL was modeled with a −100-$\mu$s best delay, i.e., inputs arrived coincidently at the left NL when the left side inputs were delayed by 100 $\mu$s with respect to the right side inputs. Left and right NL best delays were based on empirical data (Hyson et al. 1994; Overholt et al. 1992). As noted in the RESULTS, additional simulations also tested the case when the NL cells on both the left and right sides were tuned to a best ITD of 0, and thus had the *same* best-ITD tuning.

DATA ANALYSIS. Simulations showed that cell responses progressively changed over the course of hundreds of milliseconds with the inclusion of SON feedback inhibition. To capture this slow variation, cell response rates were plotted using 100-ms-long moving-averaged windows that were half-overlapped. Error bars indicate ±1 SE about the mean rate over the specified number of repetitions (each repetition used an independent stimulus sample). [Figs. 3 and 4 were generated using 10 repetitions. Figure 5 was generated using 98 repetitions (error bars are not shown for clarity). Figures 6–8 were generated using 45 repetitions.]

## RESULTS

Simulations consisted of applying bilateral auditory nerve (AN) input to the left and right sides while monitoring network cell responses. Input rate generally reflected the intensity of the auditory stimulus. Rates were either the same to the two sides (balanced inputs) or different to the two sides (imbalanced inputs). Simulations tested the network cells' responses both with and without the inclusion of SON inhibitory feedback. For a given input rate condition, two different stimulus ITDs were generally presented so that inputs from the left and right sides arrived either in-phase (i.e., coincidently) at the right NL or out-of-phase (i.e., with a 180° phase shift) at the right NL.

We present three main results. First, SON feedback inhibition maintained rate-ITD modulation in NL over a threefold range in AN input rates, whereas without SON feedback, modulation was lost at high AN rates. Second, with the inclusion of SON inhibition, rate-ITD modulation in NL improved progressively over time due to the temporal build-up of the inhibitory response. Finally, the presence of reciprocal inhibitory connections between SONs improved the robustness of rate-ITD modulation in NL on both sides of the brain stem.

### *SON inhibition and rate-ITD modulation*

Figures 3 and 4 show summary responses of all cell types in the network for low-rate (150 spikes/s to each NM and NA cell) and high-rate (450 spikes/s to each NM and NA cell)

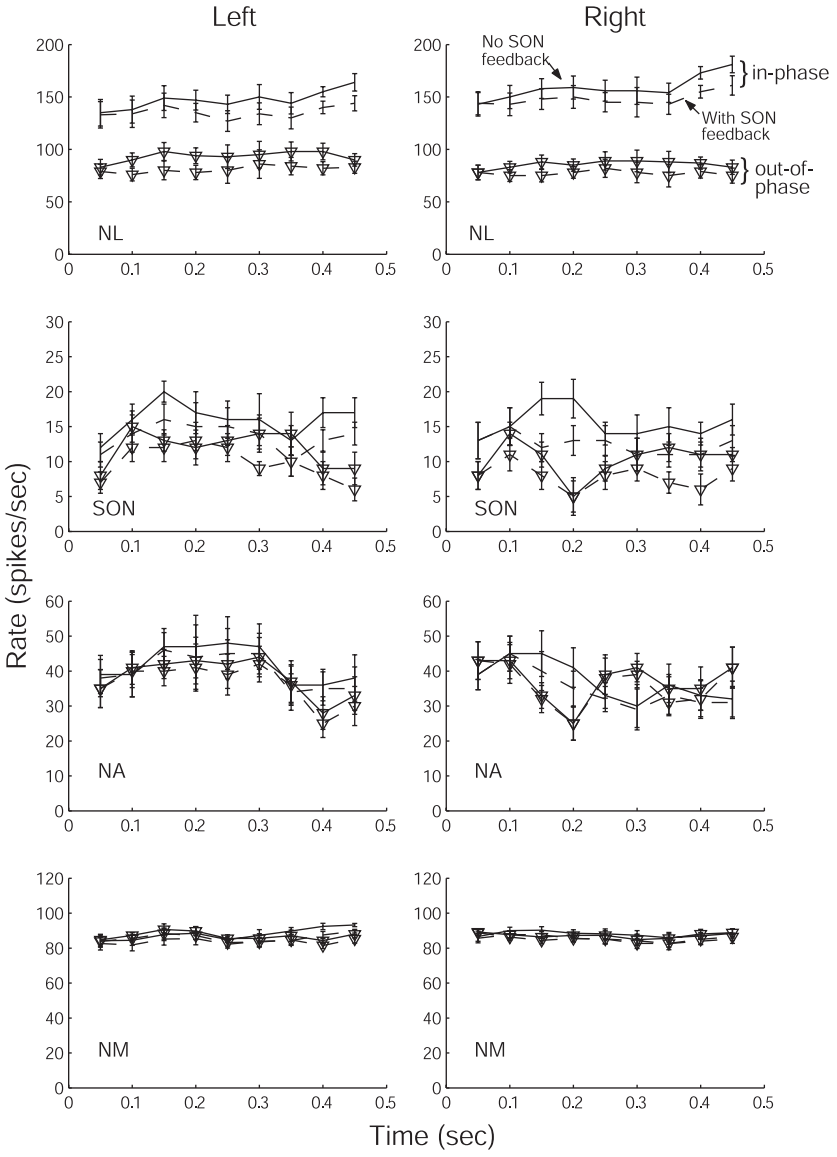


FIG. 3. Inhibition does not affect interaural time difference (ITD) modulation at low input rates. Auditory nerve input rate is 150 spikes/s to both the left and right sides. Response rate is shown for each of the modeled NL, NA, and SON cells from the left and right sides. Each NM plot shows the average response rate across the 10 NM cells on the corresponding side. Solid lines (—), cell responses without inhibitory feedback; dashed lines (- - -), cell responses to the identical stimuli set when inhibitory feedback is included. Stimuli were delivered with 1 of 2 ITDs, either so that input from the left and right NM arrived *in-phase* at the *right* NL (indicated by the points without ▽s), or so that the inputs from the left and right NM cells arrived *out-of-phase* at the *right* NL (indicated by the points with ▽s). Response asymmetries occur across the two sides because the left and right NL are tuned to different best ITDs (see METHODS).

balanced inputs, respectively. We defined the presence of rate-ITD modulation in NL as a consistently *higher* response to in-phase stimuli compared to out-of-phase stimuli over time. For low-rate inputs (Fig. 3), there was generally little difference in cell responses caused by SON feedback as indicated by the similarity of the associated solid (—) and dashed (- - -) traces. Significant rate-ITD modulation was observed in *both* the right NL (which has a best-delay equal to the in-phase stimulation delay) and the left NL (which has a best-delay that is 200 $\mu$s away from the in-phase stimulation delay) in response to low-rate inputs, both with and without the inclusion of SON feedback. In-phase responses (lines with no symbols) were consistently greater than out-of-phase responses (lines with ▽s). In contrast, with high-rate inputs of 450 spikes/s to each side (Fig. 4), rate-ITD modulation in the NL on both sides was lost without SON inhibitory feedback. In- and out-of-phase rates were both generally saturated at 600 spikes/s (—). With the inclusion of SON inhibitory feedback, however, rate-ITD modulation in NL on both sides was regained (Fig. 4, - - -). Inclusion of SON feedback generally reduced rates in all cells in the network with time (cf. Fig. 4). The resulting decrease in NM rate, together with SON directly inhibiting NL, maintained rate-ITD modulation in NL at high levels.

Figure 5 shows rate-ITD curves in the right NL for different epochs of time during the response with SON feedback. Specifically, the response rate at ITDs intermediate to the in-phase and out-of-phase delays was computed at each of the moving average windows. Responses decreased smoothly from the in-phase delay to the out-of-phase delay at a given time-point, consistent with rate-ITD curves typically observed in NL. Rate-ITD curves were symmetric for balanced inputs, both with and without inhibitory feedback (cf. Fig. 5). Small asymmetries in rate-ITD curves were initially observed to imbalanced inputs. As the influence of inhibitory feedback increased over time, NM rates on the two sides became more equal, decreasing any asymmetry initially observed in rate-ITD curves from imbalanced inputs (150, 450 spikes/s inputs were tested, data not shown).

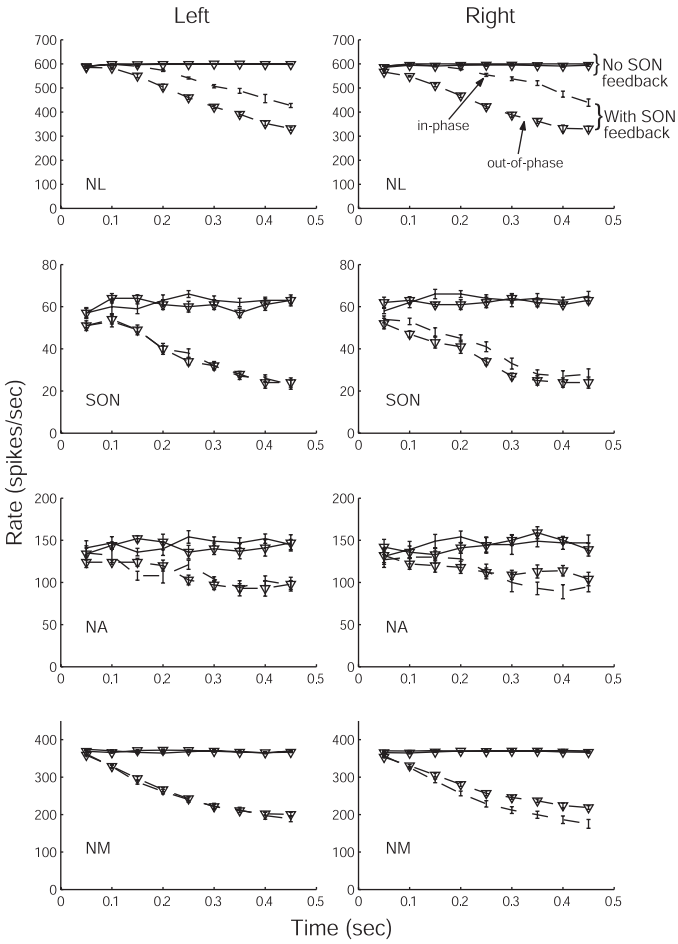


FIG. 4. Inhibition improves ITD modulation at high-input rates. Input rates are 450 spikes/s to both the left and right sides. The format is the same as Fig. 3.

The next set of simulations explored multiple stimulus levels. We introduced a percentage-of-modulation metric[3] to reflect the *relative* amount of rate-ITD modulation, which is not conveyed by absolute rate information alone. At a given timepoint, for each stimulus presentation, percentage-of-modulation is defined as the rate resulting from in-phase stimulation minus the rate resulting from out-of-phase stimulation divided by the in-phase rate and multiplied by 100. This measure better reflects the modulation. For example, the same absolute rate difference of 20 spikes/s occurs from an in-phase rate of 30 spikes/s and out-of-phase rate of 10 spikes/s as it does for an in-phase rate of 600 spikes/s and out-of-phase rate of 580 spikes/s. By contrast, the percentage-of-modulation for these two examples is 67 and 3% respectively, reflecting the larger relative amount of modulation in the former case.

Figure 6 shows the in- and out-of-phase rates for the right NL cell for several balanced and imbalanced input level conditions. Figure 7 shows the percentage-of-modulation amounts for the same conditions as Fig. 6. Without SON feedback (—), the in- and out-of-phase rates converged (Fig. 6) and the amount of rate-ITD modulation generally decreased (Fig. 7) as the average input rate to the two sides was increased (see in order, *C, D, F,* and *E* in Figs. 6 and 7). For high-input rates, modulation was reduced (e.g., Fig. 7*D*, —) or lost entirely (e.g., Fig. 7*E*, —). In contrast, with the inclusion of SON inhibitory feedback (- - -), rate-ITD modulation in NL was maintained across input rate conditions. At the highest input rates to both sides, inclusion of SON-feedback caused the most pronounced improvement in NL rate-ITD modulation, from essentially no modulation without SON feedback, to nearly 30% modulation with feedback (Fig. 7*E*, — vs. - - -). Rate-ITD modulation generally improved with the inclusion of SON feedback as input rates increased for both balanced (Fig. 7, *A, C,* and *E*) and imbalanced (Fig. 7, *B, D,* and *F*) conditions to the two sides.

Results were also obtained for a network in which the left and right NL were tuned to the *same* best ITD. These results (not shown) also demonstrated improvement in NL rate-ITD modulation to higher level balanced and imbalanced inputs with SON-feedback.

### *Rate-ITD modulation improves over time*

Our simulations indicated that SON feedback inhibition improved rate-ITD modulation in NL progressively over time

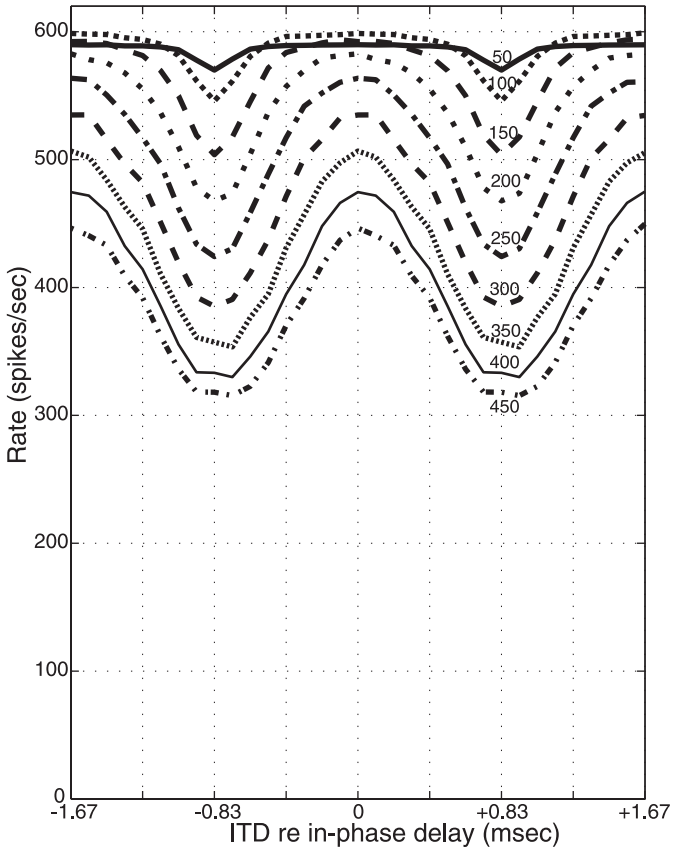


FIG. 5. Rate-ITD curves in the right NL for different epochs of time during the response. Input rate is 450 spikes/s to the 2 sides. The ITD axis has been centered with respect to the in-phase delay at the right NL. The parameter (which has units in ms) corresponds to the center of the 100-ms moving average window. For each window location, the response to each ITD over 1 period was computed. Values at negative ITDs are just the positive values reflected around the ITD = 0 point and re-plotted. At the stimulus onset, the combination of the synaptic delay and the ITD caused a total delay of 1.6 ms to the right NL; this delay caused 1 response period to be omitted from the response, which explains the slight decrease (10 spikes/s) in the response during the first window. (This slight decrease in rate at the onset can also be seen in Fig. 6.)

[3] A similar measure was used by Grau-Serrat et al. (2003) to report the degree of rate-ITD modulation in model NL.

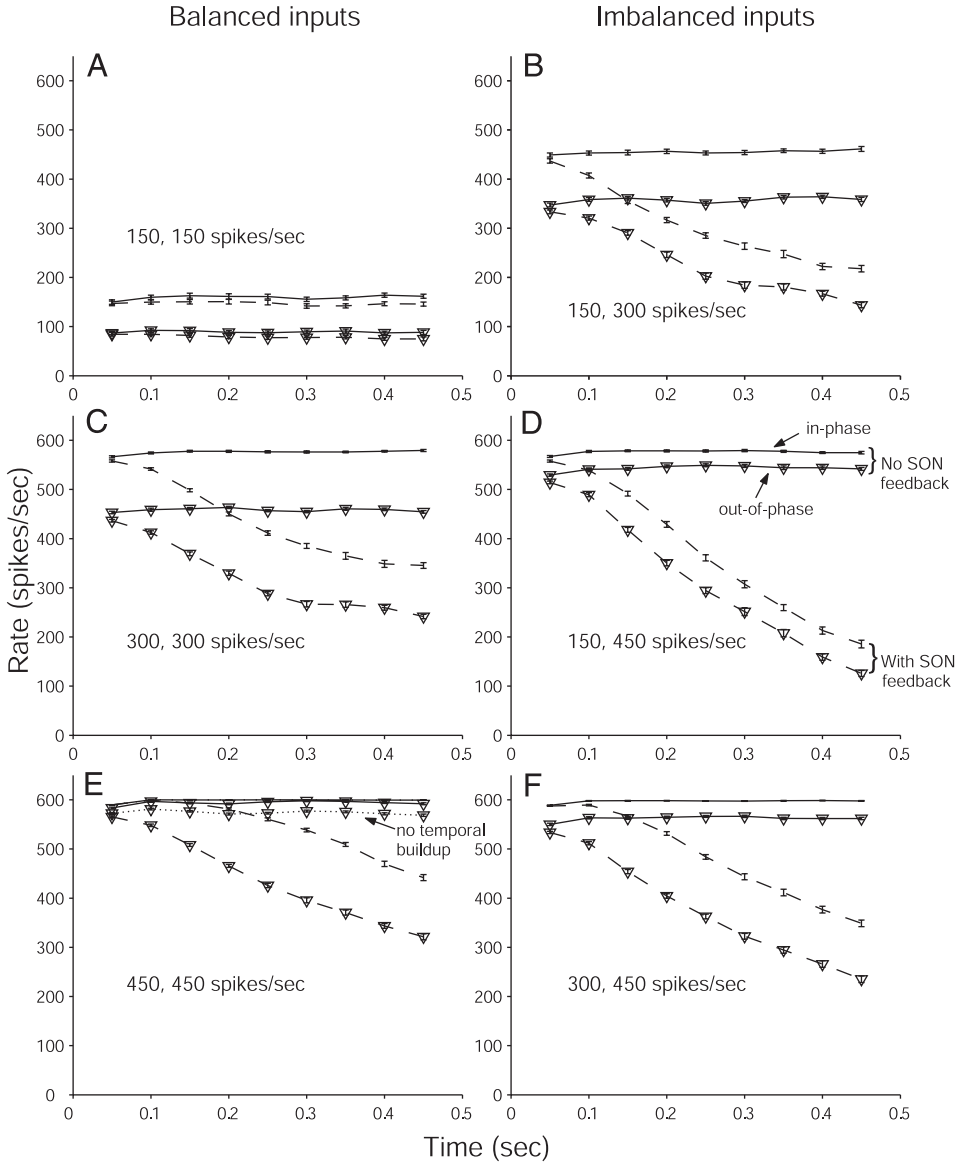


FIG. 6. Responses in the right NL for various input rate conditions, for both balanced (*left*) and imbalanced (*right*) input rates from the two sides. The additional pair of dotted lines in *E* show the responses when the SON temporal build-up mechanism is limited by setting $\tau_{\tau_m}^{ceil}$ and $\tau_{V_T}^{ceil}$ equal to 50 ms (as opposed to 1 s) for all cells (the in-phase response is essentially equal to the in-phase no-feedback response so it cannot be seen). Similar responses between the no-feedback and the no-temporal build-up with feedback cases also occurred for imbalanced inputs of 150, 450 spikes/s (data not shown).

(Figs. 6 and 7). Significant increases in the amount of rate-ITD modulation often occurred during the first 200 ms (e.g., see Fig. 7, *D, E,* and *F,* arrows). More gradual changes followed until steady-state responses were reached [after ~1 s, based on simulations with longer duration stimuli (data not shown)]. Long-lasting decreases in responses occurred because the cells in the network were interconnected and continuously influencing each other, consistent with the SON inhibitory feedback structure. Responses typically took longer to reach steady state at higher input levels (*D–F* in Figs. 6 and 7), compared with lower input levels (*A–C* in Figs. 6 and 7). This is because cells needed modulation of their parameters over a wider range for NL to show rate-ITD modulation at high levels compared with at low levels. In contrast, the response from an *isolated* adapting LIF cell model (Fig. 2) driven by relatively high, constant rates of excitatory and inhibitory input reached steady state more rapidly (within ≈0.25 s).

A key mechanism underlying the increase in rate-ITD modulation in NL over time in the network was the temporal build-up of SON inhibitory response. If SON inhibition was specified *without* the temporal build-up, such that the membrane time constant and the threshold states for all cells receiving inhibition always decayed with a *fixed* time constant of 50 ms (i.e., by fixing $\tau_{\tau_m}^{ceil}$ and $\tau_{V_T}^{ceil}$ equal to 50 ms), then the extent of rate-ITD modulation in NL was significantly reduced. The reduction in modulation was found for both large balanced input rates of 450 spikes/s to the two sides (shown in Figs. 6*E* and 7*E* by dotted lines), and for large imbalanced rates of 150, 450 spikes/s (data not shown). Rate-ITD modulation amounts with feedback but no temporal build-up were slightly larger than without-feedback conditions (compare · · · and — in Fig. 7*E*). Modulation with SON feedback but no temporal build-up, however, was significantly less than when SON feedback was specified *with* temporal build-up (compare · · · and - - - in Fig. 7*E*). Furthermore, when we tested intermediate values of $\tau_{\tau_m}^{ceil}$ and $\tau_{V_T}^{ceil}$, the maximal percentage-of-modulation monotonically increased with the recovery time-constant ceiling, while the time to reach steady state increased (100, 200, and 500 ms were

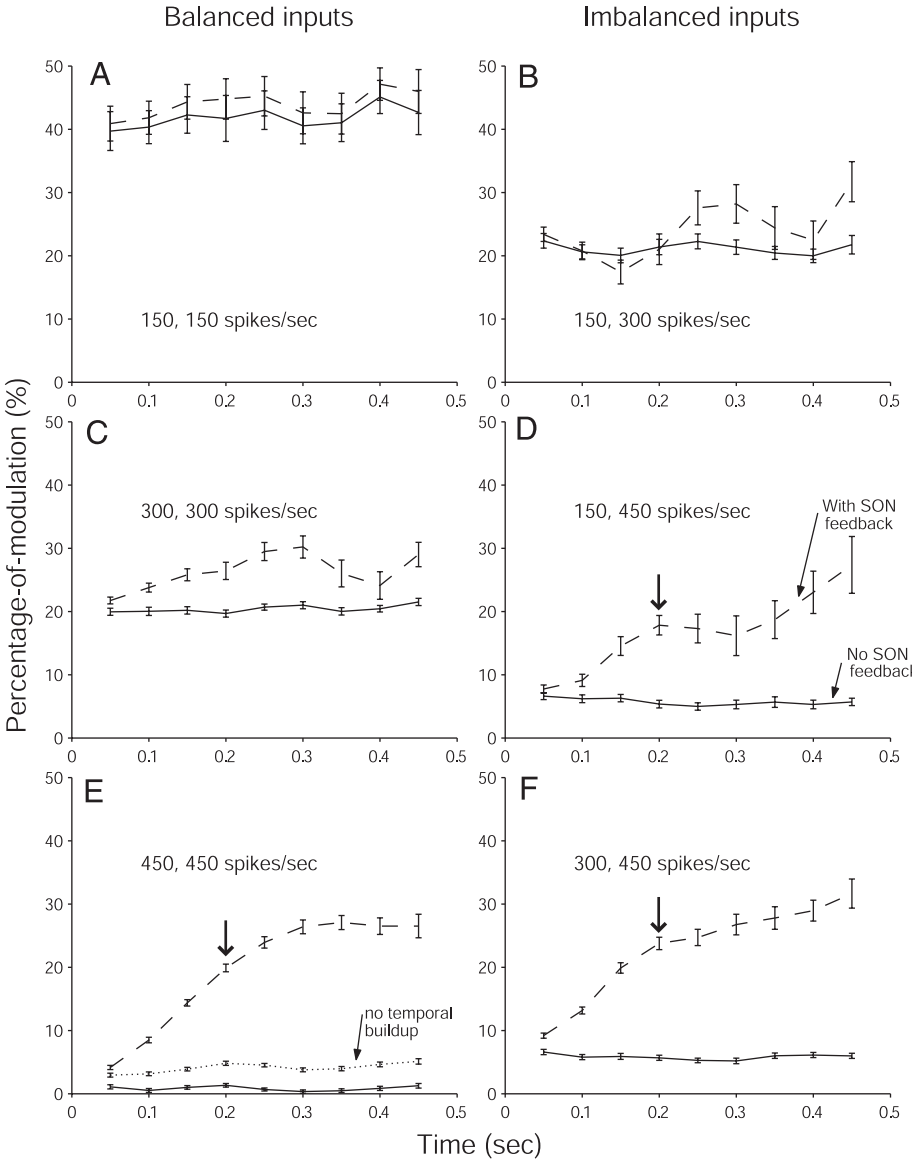


FIG. 7. Percentage-of-modulation for the same input conditions shown in Fig. 6. The additional dotted trace shown in *E* is the no-temporal-build-up with feedback case that corresponds to the same condition in Fig. 6*E*. A similar minimal improvement in modulation for the no-temporal-build-up with feedback condition compared with the no-feedback condition occurred for imbalanced inputs of 150, 450 spikes/s (data not shown).

tested, data not shown). The response for the 500-ms ceiling value actually equaled the response for the 1-s ceiling value indicating that recovery time constants did not typically exceed 500 ms in our network simulations (for both 450, 450 spikes/s and 150, 450 spikes/s, not shown). In summary, the temporal build-up of inhibition lasting hundreds of milliseconds, appeared to allow a single SON cell, despite a relatively low maximal firing rate (of ~80 spikes/s), to consistently inhibit the NL, NM, NA, and contralateral SON, which in turn, significantly improved rate-ITD modulation in NL.

### *Reciprocal inhibitory connections between SONs*

We also explored the importance of the reciprocal inhibitory connections between the ipsi- and contralateral SONs on rate-ITD modulation. These connections were found to improve rate-ITD modulation in the NL on *both* sides of the brain stem. Figure 8 shows rate responses and modulation amounts in both the right and left NL cells for an input rate-imbalanced case for three SON feedback conditions: no feedback, feedback with no reciprocal (SON-to-SON) connections (i.e., ipsilateral only feedback), and full SON-feedback (i.e., including reciprocal connections). With full feedback inhibition, modulation was consistently maintained over time in both the right and the left NL (Fig. 8, all panels, thin dashed lines). With no SON-to-SON reciprocal inhibitory connections, however, rate-ITD modulation was reduced in NL on both sides —especially in the NL on the side not tuned to the stimulus ITD (Fig. 8, *left*, thick dashed lines). This ipsilateral-only inhibitory condition caused a dip in the modulation over time, driven to the extent where the modulation at 0.35 s was significantly reduced (right NL) and lost entirely (left NL). Without the reciprocal inhibitory SON projections, a reduction in rate-ITD modulation was also found for level-balanced cases of 300, 300 spikes/s and 450, 450 spikes/s (data not shown). A decrease in the regulation of SON feedback arising from the ipsilateral only feedback condition reduced the in-phase response excessively, ultimately reducing modulation.

Because it is not conclusively known whether the SON-to-SON projections are inhibitory (cf. Burger et al. 2005; Lachica

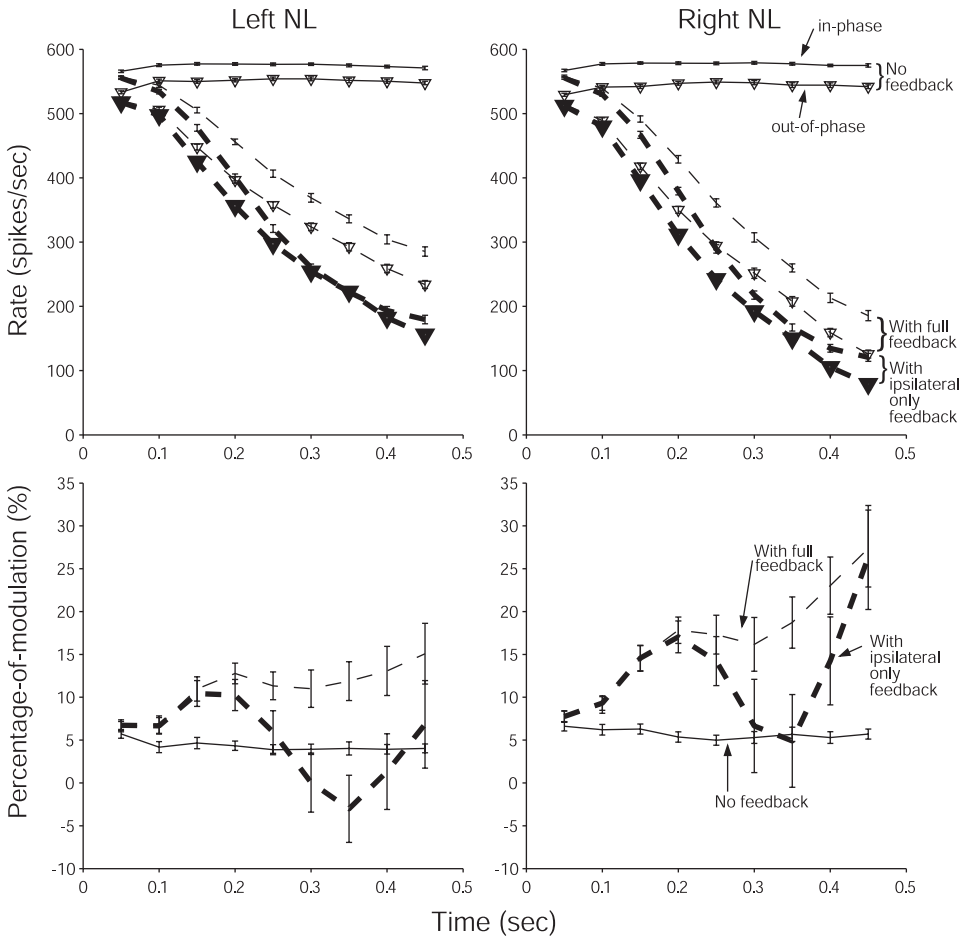


FIG. 8. Response rates and percentage-of-modulation in the left and right NL under three different configurations of SON feedback inhibition. Input rates are 150 spikes/s to the left side and 450 spikes/s to the right side. The parameter is the specific SON inhibitory feedback connectivity for three conditions: no inhibition, ipsilateral only inhibition (i.e., no inhibitory connections between the two SON in Fig. 1), and full feedback inhibition as shown in Fig. 1.

et al. 1994), we conducted additional simulations in which the reciprocal connections between SONs were specified to be excitatory. Rate-ITD modulation was generally poor under these excitatory-coupled SON conditions. For the 150, 450 spikes/s case, an even greater reduction in rate-ITD modulation was observed in both NL for excitatory connections between the SONs compared with the no-connections between the SONs case (data not shown). Furthermore, with excitatory reciprocal connections, while consistent modulation was maintained in the right NL in response to high-level balanced-inputs of 450, 450 spikes/s, convergence of in- and out-of-phase rates occurred in the left NL, reducing modulation essentially to zero (data not shown). Modulation was maintained in the left NL, however, with the presence of *inhibitory* connections between the SONs (Fig. 4, *top left,* - - -). Reciprocal inhibitory connections between the two SONs therefore appear beneficial in maintaining rate-ITD modulation in NL, both temporally, over the entire stimulus duration, and spatially, across the two sides of the brain.

## DISCUSSION

The avian auditory brain stem network is composed of the NL, NM, NA, and SON. The SON, which is excited by NL and NA, exerts feedback inhibition on the NL, NM, and NA, and likely on the contralateral SON as well. We analyzed this network circuit using computational modeling. Several key results were found.

Overall, the influence of SON inhibitory feedback on the avian brain stem circuit expands the dynamic range of the ITD coding system to sound level. SON inhibitory feedback is most beneficial in maintaining ITD sensitivity[4] in NL at high levels, where ITD sensitivity is otherwise lost when feedback is not included. Sensitivity to ITD is maintained for both balanced and imbalanced levels to the two sides, with the inclusion of SON inhibitory feedback. When the empirically observed temporal build-up of the SON inhibitory response is not incorporated in the network model, ITD sensitivity decreases sharply. Further, the presence of reciprocal inhibitory connections between the two SONs increases the stability of ITD coding in the NL on both sides of the brain.

SON feedback inhibition generally maintains rate-ITD sensitivity in NL by preserving the coincidence detecting ability of NL on the inputs coming from the left and right NM. SON contributes to robust coincidence detection in NL through a dual mechanism: indirectly, by inhibiting NM, reducing the afferent rate to NL, and directly, by inhibiting NL itself.

### *Feedback inhibition*

A previous model by Peña and colleagues (1996) included only *forward* connectivity from SON to a single NL cell model. We constructed a bilateral network model with feed-

[4] In this DISCUSSION, we assume that the relative extent of rate-ITD modulation in NL reflects the sensitivity of NL to changes in ITD.

back that includes both forward and *backward* connectivity observed in bird anatomy. Both models demonstrate that forward connections provide sound-level-dependent inhibition, maintaining ITD sensitivity in NL across level. Both models also indicate that inhibition causes the greatest improvement in ITD sensitivity at the highest sound levels, where sensitivity is most reduced without inhibition. While inhibition improves ITD sensitivity across sound level in both feedback and forward models, we highlight two additional properties gained with feedback connectivity.

First, the reciprocal inhibitory connections between SONs improve ITD coding in NL. Including inhibitory coupling between the left and right SONs, in addition to each of the left- and right-side SON inhibitory loops, increases the robustness of ITD coding, both spatially (across the NL in the two hemifields), and temporally (over the entire stimulus duration). With SON inhibition to the ipsilateral targets only (or when excitatory connections are specified between the left and right SON cells), excessive inhibition can occur, significantly reducing ITD sensitivity in NL. In the actual physiological system, inhibitory connections between the two SON nuclei could serve to improve the ITD coding stability in NL by regulating the amount of inhibition delivered to the two sides. In vitro physiology in conjunction with neuroanatomical tracing and neurotransmitter-receptor staining studies could test whether the SON-to-SON projections are inhibitory and GABAergic, as predicted by our model.

Second, the model demonstrates that the feedback connectivity from NL to SON can impart ITD sensitivity in the SON inhibition. As a result, the SON response can be higher during in- versus out-of-phase stimulation (see Fig. 4, right SON, - - -). Consequently, NM response is more inhibited, and therefore lower during in- versus out-of-phase stimulation to the NL (see Fig. 4, right NM, - - -). These predictions depend on the small number of neurons and point-to-point connectivity specified in our network model. In the actual system, any potential ITD sensitivity observed in NM would hypothetically decrease as the amount of convergence increased from different best ITD-tuned NL cells to a single SON cell, thus smearing out ITD sensitivity in SON and therefore NM. Similarly, greater convergence from SON cells with different ITD dependencies to a single NM cell would also presumably reduce any ITD sensitivity in NM. The fact that the projection from SON to NM appears to be broadly tuned as opposed to tonotopic (Burger et al. 2005) could be consistent with the possibility that multiple SON cells converge onto a single NM cell. Nevertheless, our simulations provide rationale to investigate ITD sensitivity in SON and NM in vivo.

COMPARISON WITH OTHER MODELS WITH INHIBITION. Forward inhibition has been demonstrated in the mammalian medial superior olive (MSO) (Brand et al. 2002; Grothe and Sanes 1994; Smith et al. 2000). Because the avian inhibitory feedback circuit appears suited to maintain ITD sensitivity over variations in sound level, the mammalian inhibitory system may also play a similar role. Assuming that the discharge rate of the mammalian inhibitory input is dependent on sound level, greater inhibition at higher levels could hypothetically protect ITD sensitivity in the MSO (cf. Reed and Durbeck 1995). One difference with mammalian models that have implemented phase-locked forward inhibition is that inhibition can influence a shift in the rate-ITD curve (Brand et al. 2002; Zhou et al. 2005). Rate-ITD curves, however, do not shift with inhibitory feedback in our model of the avian system.

### *Dynamic effects of inhibition*

Long-lasting inhibitory responses (i.e., ≥50 ms) have been demonstrated in vitro in the chicken. The duration of the SON inhibitory response increased with greater input (Lu and Trussell 2000; Monsivais et al. 2000; Yang et al. 1999), with build-up extending to 1 s in NL (Yang et al. 1999). Also the EPSPs measured in single SON cells were relatively slow, on the order of 40 ms (Yang et al. 1999). We incorporated these empirically observed attributes into our network model and found that cell rates generally decrease over hundreds of milliseconds, while rate-ITD sensitivity in NL progressively increased.

COMPARISON WITH SYNAPTIC DEPRESSION. The improvement in rate-ITD sensitivity demonstrated in this study is much slower than that found in a model of NL that incorporated synaptic depression observed in the chick NM to NL synapse (Cook et al. 2003). The time course of depression observed in the NM-to-NL synapse was on the order of tens of milliseconds (Cook et al. 2003; Kuba et al. 2002). In the functioning system, we speculate that synaptic depression may operate on a short-term time scale in conjunction with SON inhibition operating on a longer-term time scale.

COMPARISON WITH IN VIVO DATA. Our simulations are in general agreement with in vivo findings in owl that GABA sharpens the ITD sensitivity of NL (Fujita and Konishi 1991; Takahashi and Konishi 2002). The responses in our model, however, are slower than those observed in owl (Fujita and Konishi 1991; Peña et al. 1996; Viete et al. 1997; Takahashi and Konishi 2002). In the owl data, steady-state responses appear to have been reached in response to 100-ms stimuli (e.g., see Peña et al. 1996; Fig. 1, B and C). We propose the following five possibilities for the time course differences between the model and these in vivo data: 100-ms stimuli may have been too short for a possible slow component to be seen in vivo, species differences between the owl and chicken, anesthesia may have influenced the in vivo responses, the low temperature (i.e., room temperature) that in vitro experiments were conducted, on which we based our model parameters, and our simulations were always started with the same set of initial values of states. The last two points are discussed in the following paragraphs.

Our model parameters were based on in vitro experiments conducted at room temperature (Yang et al. 1999). Lower temperatures could increase the duration of effects observed in vitro compared with those occurring in vivo (Funabiki et al. 1998; Kuba et al. 2003). For example, Funabiki and colleagues (1998) showed that the time course of EPSPs in NL was significantly shorter at in-vivo-like temperatures compared with room temperature, particularly when GABA was applied. It is possible that the temporal build-up of SON inhibition may also be reduced at body temperatures. However, temporal build-up was also demonstrated in slice at in-vivo-like temperatures of 35°C (Lu and Trussell 2000). Moreover, Lu and Trussell (2000) in the same study demonstrated evoked inhibitory plateau currents that lasted a

few hundred milliseconds [see Lu and Trussell 2000; Fig. 1(iv)]. The recovery time constants specified in our model that control the dynamics of the membrane time constant and voltage threshold in model cells rarely exceeded 500 ms. A 500-ms upper limit of inhibitory build-up seems consistent with the hundreds of millisecond long plateau currents observed empirically at 35°C.

Our simulations used the same default set of initial values at the start of each stimulus presentation (independent of input history or stimulus level). In the functioning system with continuous sound exposure and the presence of spontaneous activity, the SON feedback system may be continually "primed," allowing the SON to provide more or perhaps less inhibition in response to high or low sound levels. The physiological system may be in an "optimal ready state" that is able to respond efficiently across a range of input levels. Response times in vivo may therefore be faster than those predicted from in vitro conditions.

Physiological studies could further elucidate the effects of SON GABAergic inhibition, specifically on NA, NM, and possibly on contralateral SON. Of interest would be whether the magnitudes and durations of the observed inhibitory responses are on the order of those observed in vitro in NL by Yang and colleagues (1999). Moreover, in vivo studies in chicken auditory brain stem using multibarrel recording electrodes with bicuculline would be useful to compare baseline responses (which would presumably be observed *with* physiological SON GABAergic inhibition intact), with responses obtained when bicuculline is administered (to block GABAergic effects). Results could be compared with similar experiments in owl (Fujita and Konishi 1991). Based on our simulations, response time courses could speed up if GABAergic responses are blocked.

TEMPORAL BUILD-UP AND DYNAMIC RANGE. Our simulations specify a discharge rate range for SON that is compatible with that observed in vitro by Yang and colleagues (1999). The inclusion of the empirically observed temporal build-up of inhibitory response significantly increases the amount of rate-ITD modulation observed in NL. This finding could suggest that the temporal build-up of inhibition may be a mechanism by which a single SON cell, despite a relatively low firing rate, can provide significant inhibition/modulation on its targets. Lu and Trussell (2000) demonstrated that temporal build-up of inhibition occurred as a result of the asynchronous synaptic release of GABA as a consequence of increased SON fiber stimulation. Our model suggests that the temporal build-up of inhibition significantly increases the ITD sensitivity of NL at high levels. SON fiber synaptic specializations could therefore underlie the increase in the dynamic range of the ITD coding system.

### *Study limitations*

One limitation of our study is that we specified SON inhibition to modulate a target cell's membrane time constant and threshold without affecting its membrane voltage. On the one hand, GABAergic input from SON has been demonstrated to be depolarizing (Lu and Trussell 2001; Monsivais and Rubel 2001), even causing occasional spiking (Lu and Trussell 2001; Lu et al. 2005). On the other hand, the GABA released from SON fibers could be limited by presynaptic $GABA_B$ receptor activation, which can suppress GABA-evoked discharges (Lu et al. 2005). Further, because GABA-induced spiking was most reliable only at the onsets of (phasic) input trains (Lu and Trussell 2001), we suspect a negligible discharge rate to steady-state inputs like those used in the present study. Moreover, the effect of inhibition on membrane voltage may not be as critical as the absolute conductance change (i.e., the shunting effect) of the inhibitory synapse itself. A physiologically detailed model of NL showed similar levels of ITD sensitivity regardless of whether the inhibitory input from SON was specified to be depolarizing or hyperpolarizing (Grau-Serrat et al. 2003). Future empirical and modeling studies could further explore the impact of SON-induced depolarization, particularly under phasic stimulation conditions.

A second limitation of our study is that the leaky-integrate-and-fire (LIF)-type cell models used do not contain ion channels (such as low-threshold potassium channels) or dendrites, both of which can reduce response to less-coincident (e.g., out-of-phase) inputs (cf. Agmon-Snir et al. 1998; Cook et al. 2003; Dasika 2004; Grau-Serrat et al. 2003; Reyes et al. 1996; Svirskis et al. 2003, 2004). Ion channels and dendrites may help maintain ITD sensitivity in NL by keeping in-phase responses consistently greater than out-of-phase responses. LIF models, on the other hand, can exhibit "reverse-modulation" under certain high-level stimulation conditions, such that the out-of-phase response can actually *exceed* the in-phase response (cf. Peña et al. 1996; Reed and Durbeck 1995). The fact that LIF models can demonstrate reverse-modulation may actually provide a more stringent test of SON feedback inhibition. The out-of-phase response needs to be reduced significantly, while the in-phase response should not be excessively reduced, to achieve rate-ITD modulation, under stimulus conditions that induce reverse-modulation. We found that the inclusion of SON inhibitory feedback in the network model could change responses in NL from significant reverse-modulation to modulation [data not shown; percentage-of-modulation without SON feedback was $-67\%$; percentage-of-modulation with SON feedback was $+18\%$; $f = 450$ Hz; $R = 450$ spikes/s to the two sides; stimulus length $= 2$ s (steady-state responses occurred by $\sim 1$ s)]. SON inhibition therefore appears to be both potent and adaptable, providing an appropriate amount of feedback to achieve ITD sensitivity in NL.

### *Concluding remarks*

The avian brain stem network embodying SON inhibitory feedback demonstrates robust ITD coding across sound-level. The effects of feedback inhibition are similar to those derived from forward inhibition, with added stability.

Future studies could test the effects of SON inhibitory feedback combined with the inclusion of synaptic depression (cf. Cook et al. 2003). Specific contributions of each mechanism, as well as net effects due to both mechanisms, should be determined. We speculate that the ITD coding system would be most robust when both SON network inhibition *and* synaptic depression are jointly incorporated. Both mechanisms are presumably acting in parallel in the functioning organism, albeit possibly at different time scales—with depression adjusting the synaptic strength within milliseconds, and SON inhibition providing long-term modulation over hundreds of millisec-

onds. Such studies would further increase our understanding of how neural specializations expand the dynamic range of the auditory system.

## APPENDIX

Here we provide the derivation of the expression for the membrane voltage in the adapting LIF model shown in *Eq. 3*. To derive the expression for the membrane voltage since the time immediately after the last input event ($t_k^+$), and before the time of the next input event, we start with *Eq. 2*

$$\frac{dV_m(t)}{dt} = \frac{-V_m(t)}{\tau_m(t)} = \frac{-V_m(t)}{\underbrace{(\tau_m(t_k^+) - \tau_m^0)\exp\left(\frac{-(t-t_k^+)}{\tau_{\tau_m}(t_{inh,rec}^+)}\right) + \tau_m^0}_{\tau_m(t)}} \quad (A1)$$

*Eq. A1* is rearranged and integrated from $t_k^+$ to $t$ as shown in *Eq. A2*

$$\int_{t_k^+}^{t} \frac{dV_m(t')}{V_m(t')} = \frac{-\tau_{\tau_m}(t_{inh,rec}^+)}{\tau_m^0} \int_{t_k^+}^{t} \frac{\frac{1}{\tau_{\tau_m}(t_{inh,rec}^+)}\exp\left(\frac{t'-t_k^+}{\tau_{\tau_m}(t_{inh,rec}^+)}\right)}{\exp\left(\frac{t'-t_k^+}{\tau_{\tau_m}(t_{inh,rec}^+)}\right) + \frac{(\tau_m(t_k^+) - \tau_m^0)}{\tau_m^0}} dt' \quad (A2)$$

resulting in

$$\ln\frac{V_m(t)}{V_m(t_k^+)} = \ln\left[\left(\frac{\exp\left(\frac{t-t_k^+}{\tau_{\tau_m}(t_{inh,rec}^+)}\right) + \frac{(\tau_m(t_k^+) - \tau_m^0)}{\tau_m^0}}{\frac{\tau_m(t_k^+)}{\tau_m^0}}\right)^{\frac{-\tau_{\tau_m}(t_{inh,rec}^+)}{\tau_m^0}}\right] \quad (A3)$$

*Eq. A3* can be rewritten as

$$\frac{V_m(t)}{V_m(t_k^+)} = \left[\frac{\frac{\tau_m(t_k^+)}{\tau_m^0}\exp\left(\frac{-(t-t_k^+)}{\tau_{\tau_m}(t_{inh,rec}^+)}\right)}{1 + \frac{(\tau_m(t_k^+) - \tau_m^0)}{\tau_m^0}\exp\left(\frac{-(t-t_k^+)}{\tau_{\tau_m}(t_{inh,rec}^+)}\right)}\right]^{\frac{\tau_{\tau_m}(t_{inh,rec}^+)}{\tau_m^0}} \quad (A4)$$

which can be rewritten as *Eq. 3*.

## ACKNOWLEDGMENTS

We thank Drs. Michael Burger and Edwin Rubel for valuable comments on this manuscript and for sharing insight and data on the avian auditory brain stem. We also thank Dr. Wil Howitt for helpful advice on the computational implementation of the simulations. We thank the two anonymous reviewers and Dr. Catherine Carr, whose comments greatly improved this paper.

## GRANTS

This work was supported by National Institutes of Health Grants DC-00100, NS-24425, and DC-01641.

## REFERENCES

**Agmon-Snir H, Carr CE, and Rinzel J.** The role of dendrites in auditory coincidence detection. *Nature* 393: 268–272, 1998.

**Blauert J.** *Spatial Hearing: The Psychophysics of Human Sound Localization* (revised ed.). Cambridge, MA: The MIT Press, 1997.

**Brand A, Behrend O, Marquardt T, McAlpine D, and Grothe B.** Precise inhibition is essential for microsecond interaural time difference coding. *Nature* 30: 543–547, 2002.

**Burger RM, Cramer KS, Pfeiffer JD, and Rubel EW.** Avian superior olivary nucleus provides divergent inhibitory input to parallel auditory pathways. *J Comp Neurol* 481: 6–18, 2005.

**Carr CE and Konishi M.** A circuit for detection of interaural time differences in the brain stem of the barn owl. *J Neurosci* 10: 3227–3246, 1990.

**Colburn HS, Zhou Y, and Dasika VK.** Inhibition in models of coincidence detection. In: *Auditory Signal Processing: Physiology, Psychoacoustics, and Models,* edited by Pressnitzer D, de Cheveigne A, McAdams S, and Collet L. New York: Springer, 2004, p. 299–305.

**Cook DL, Schwindt PC, Grande LA, and Spain WJ.** Synaptic depression in the localization of sound. *Nature* 421: 66–70, 2003. (Corrigenda, *Nature* 423: 197, 2003

**Dasika VK.** Dendritic models and the influence of spatial coupling on time-delay sensitivity. In: *Models of Auditory Brainstem Coincidence-Detector Neurons* (PhD dissertation). Boston, MA: Boston University, 2004, p. 67–101

**Dayan P and Abbott LF.** Mathematical appendix. In: *Theoretical Neuroscience: Computational and Mathematical Modeling of Neural Systems,* edited by Sejnowski TJ and Poggio T. Cambridge, MA: The MIT Press, 2001, p. 404–405.

**Fujita I and Konishi M.** The role of GABAergic inhibition in processing of interaural time difference in the owl's auditory system. *J Neurosci* 11: 722–739, 1991.

**Funabiki K, Koyano K, and Ohmori H.** The role of GABAergic inputs for coincidence detection in the neurons of nucleus laminaris of the chick. *J Physiol* 508: 851–869, 1998.

**Goldberg JM and Brown PB.** Response of binaural neurons of dog superior olivary complex to dichotic tonal stimuli: some physiological mechanisms of sound localization. *J Neurophysiol* 32: 613–636, 1969.

**Grau-Serrat V, Carr CE, and Simon JZ.** Modeling coincidence detection in nucleus laminaris. *Biol Cybern* 89: 388–396, 2003.

**Grothe B.** New roles for synaptic inhibition in sound localization. *Nat Rev Neurosci* 4: 540–550, 2003.

**Grothe B and Sanes DH.** Synaptic inhibition influences the temporal coding properties of medial superior olivary neurons: an in vitro study. *J Neurosci* 14: 1701–1709, 1994.

**Hyson RL, Overholt EM, and Lippe WR.** Cochlear microphonic measurements of interaural time differences in the chick. *Hear Res* 81: 109–118, 1994.

**Hyson RL, Reyes AD, and Rubel EW.** A depolarizing inhibitory response to GABA in brainstem auditory neurons of the chick. *Brain Res* 677: 117–126, 1995.

**Jeffress LA.** A place theory of sound localization. *J Comp Physiol Psychol* 41: 35–39, 1948.

**Joris PX, Carney LH, Smith PH, and Yin TC.** Enhancement of neural synchronization in the anteroventral cochlear nucleus. I. Responses to tones at the characteristic frequency. *J Neurophysiol* 71: 1022–1036, 1994.

**Kuba H, Koyano K, and Ohmori H.** Synaptic depression improves coincidence detection in the nucleus laminaris in brainstem slices of the chick embryo. *Eur J Neurosci* 15: 984–990, 2002.

**Kuba H, Yamada R, and Ohmori H.** Evaluation of the limiting acuity of coincidence detection in nucleus laminaris of the chicken. *J Physiol* 552: 611–620, 2003.

**Lachica EA, Rübsamen R, and Rubel EW.** GABAergic terminals in nucleus magnocellularis and laminaris originate from the superior olivary nucleus. *J Comp Neurol* 348: 403–418, 1994.

**Lu Y, Burger RM, and Rubel EW.** $GABA_B$ receptor activation modulates $GABA_A$ receptor-mediated inhibition in chicken nucleus magnocellularis neurons. *J Neurophysiol* 93: 1429–1438, 2005.

**Lu T and Trussell LO.** Inhibitory transmission mediated by asynchronous transmitter release. *Neuron* 26: 683–694, 2000.

**Lu T and Trussell LO.** Mixed excitatory and inhibitory GABA-mediated transmission in chick cochlear nucleus. *J Physiol* 535: 125–131, 2001.

**Monsivais P and Rubel EW.** Accommodation enhances depolarizing inhibition in central neurons. *J Neurosci* 21: 7823–7830, 2001.

**Monsivais P, Yang L, and Rubel EW.** GABAergic inhibition in nucleus magnocellularis: implications for phase locking in the avian auditory brainstem. *J Neurosci* 20: 2954–2963, 2000.

**Overholt EM, Rubel EW, and Hyson RL.** A circuit for coding interaural time differences in the chick brainstem. *J Neurosci* 12: 1698–1708, 1992.

**Peña JL, Viete S, Albeck Y, and Konishi M.** Tolerance to sound intensity of binaural coincidence detection in the nucleus laminaris of the owl. *J Neurosci* 16: 7046–7054, 1996.

**Raman IM, Zhang S, and Trussell LO.** Pathway-specific variants of AMPA receptors and their contribution to neuronal signaling. *J Neurosci* 14: 4998–5010, 1994.

**Reed MC and Durbeck L.** Delay lines and auditory processing. *Comments Mod Biol C Comments Theor Biol* 3: 441–461, 1995.

**Reyes AD, Rubel EW, and Spain WJ.** Membrane properties underlying the firing of neurons in the avian cochlear nucleus. *J Neurosci* 14: 5352–5364, 1994.

**Reyes AD, Rubel EW, and Spain WJ.** In vitro analysis of optimal stimuli for phase-locking and time-delayed modulation of firing in avian nucleus laminaris neurons. *J Neurosci* 16: 993–1007, 1996.

**Smith AJ, Owens S, and Forsythe ID.** Characterisation of inhibitory and excitatory postsynaptic currents of the rat medial superior olive. *J Physiol* 529: 681–698, 2000.

**Soares D, Chitwood RA, Hyson RL, and Carr CE.** Intrinsic neuronal properties of the chick nucleus angularis. *J Neurophysiol* 88: 152–162, 2002.

**Sullivan WE and Konishi M.** Segregation of stimulus phase and intensity coding in the cochlear nucleus of the barn owl. *J Neurosci* 4: 1787–1799, 1984.

**Svirskis G, Dodla R, and Rinzel J.** Subthreshold outward currents enhance temporal integration in auditory neurons. *Biol Cybern* 89: 333–340, 2003.

**Svirskis G, Kotak V, Sanes DH, and Rinzel J.** Sodium along with low-threshold potassium currents enhance coincidence detection of subthreshold noisy signals in MSO neurons. *J Neurophysiol* 91: 2465–2473, 2004.

**Takahashi Y and Konishi M.** Manipulation of inhibition in the owl's nucleus laminaris and its effects on optic tectum neurons. *Neuroscience* 111: 373–378, 2002.

**Tuckwell H.** The Lapicque model of the nerve cell. In: *Introduction to the Theoretical Neurobiology.* Cambridge: Cambridge, 1988, vol. 1, p. 85–123.

**Viete S, Peña JL, and Konishi M.** Effects of interaural intensity difference on the processing of interaural time difference in the owl's nucleus laminaris. *J Neurosci* 17: 1815–1824, 1997.

**Warchol ME and Dallos P.** Neural coding in the chick cochlear nucleus. *J Comp Physiol [A]* 166: 721–734, 1990.

**Yang L, Monsivais P, and Rubel EW.** The superior olivary nucleus and its influence on nucleus laminaris: a source of inhibitory feedback for coincidence detection in the avian auditory brainstem. *J Neurosci* 19: 2313–2325, 1999.

**Zhou Y and Colburn HS.** A neural model of an MSO neuron. *Abstracts of the Midwinter Research Meeting/Association for Research in Otolaryngology* 1514, 2003. http://www.aro.org/archives/2003/2003_1514.html

**Zhou Y, Carney LH, and Colburn HS.** A model for ITD sensitivity in the MSO: Interaction of excitatory and inhibitory synaptic inputs, channel dynamics, and cellular morphology. *J Neurosci* 25: 3046–3058, 2005.